Integrated RFIC On-Chip and GPS Antenna with Human Body for Wrist and Wearable Communication Applications

Wen Cheng Lai and Jhin Fang Huang

Department of Electronic Engineering
National Taiwan University of Science and Technology
wenlai@mail.ntust.edu.tw

Abstract ─ A GPS and Miracast RFIC-on-chip antenna in 0.18 um CMOS 1p6M process is presented. The HFSS 3-D EM simulator is employed for design simulation. A printed 1.575 GHz and 2.4 GHz antenna has been realized by using the CMOS RFIC-on-chip. The measured VSWR is less than 2 from 1.575 GHz and 2.4- to 2.483-GHz. This propose super quadric combo antenna in free space, electromagnetic coupling between super quadric antenna and human body and rectangular antenna for wrist watch type wireless communication applications. The measured phase distribution of the input impedance is quite linear and the H-plane patterns are almost omnidirectional and field tried GPS integration. In addition, in order to improve the way controlling this provide switch by software, a novel circuit structure which will control antenna pattern switching automatically by hardware is also developed for wireless healthcare and mobile biomedical application. RFIC-on-chip GPS and Miracast antenna also merger T/R-Switch design on single chip solution for 2.4GHz CMOS transceiver RF front-end. The old man can monitor healthcare and transfer to health center or passive devices by Miracast with software and show GPS location for wearable ambulatory application.

Index Terms ─ Chip antenna, GPS, wearable communication, wrist and wireless application.

I. INTRODUCTION

Wrist wearable ambulatory healthcare and mobile biomedical application for old man demand. The 1.575 GHz and 2.4 GHz CMOS RFIC on-Chip antenna and T/R-Switch for wireless application [1] silicon-germanium (SiGe) HBT processing 1.575 GHz and 2.4 GHz band antenna and merger T/R-Switch design as shown in Fig. 1, [2], [3]. This analysis has including super quadric combo antenna in free space, electromagnetic coupling between super quadric antenna and human body and rectangular antenna for wrist watch type wireless communication applications. CMOS standard processing FET based T/R switch that insertion loss more large and power handing capability performance low. But now low power transceiver develop insertion loss low and FET based T/R switch is more importance [4], [5]. This flexible proximate d antenna has switch by software, and develop a novel circuit structure controlling antenna pattern switching automatically by hardware.

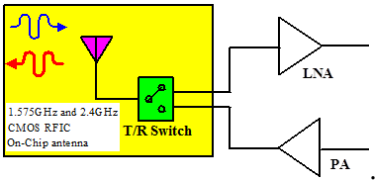

Fig. 1. The structure of 1.575 GHz and 2.4 GHz CMOS transceiver front –end Antenna and T/R-Switch.

II. GPS AND MIRACAST RFIC-ON-CHIP ANTENNA

The proposed 1.575 GHz and 2.4-GHz RFIC-on-chip antenna with T/R-Switch in 0.18 um CMOS 1p6M process is designed and based on the mender line by loop type. The chip area is 1.21 (1.1mm×1.1mm) mm^2 as shown in Fig. 2. The simulated VSWR of the single RFIC-on-chip antenna is less than 2 from 1.575 GHz and 2.4- to 2.483-GHz as shown in Fig. 3 and Fig. 4. At antenna part of M6 layer the trace width is 30mm on 0.75mm x 1.1mm area. M1~M6 metal layer are grounding to M3~M6 layer by via. The antenna paths are M1 and M2 including area 0.27mm x 0.94mm and extend 0.07mm trace to meet VSWR is less than 2 from 1.575 GHz and 2.4- to 2.483-GHz. M5 layer is shielding area 0.47mm x 0.67mm to metal grounding. The distance is 30μm between pad area 0.2mm x 0.1mm and grounding can support measured VSWR on wafer measurement by GS testing finger as pad used multi-layers and multi-via. The T/R-switch is expected to be integrated with the front-end circuits into the chip that area is 0.15mm x 1.1mm as shown in Fig. 5 [6].

In the monolithic switching system, this device can operate two switching status by controlling with a low

Submitted On: September 29, 2015
Accepted On: October 1, 2015

forward voltage drop and a very fast switching action. Switching radiation pattern is demonstrated such that the fading effect due to multipath propagations could be avoided [7].

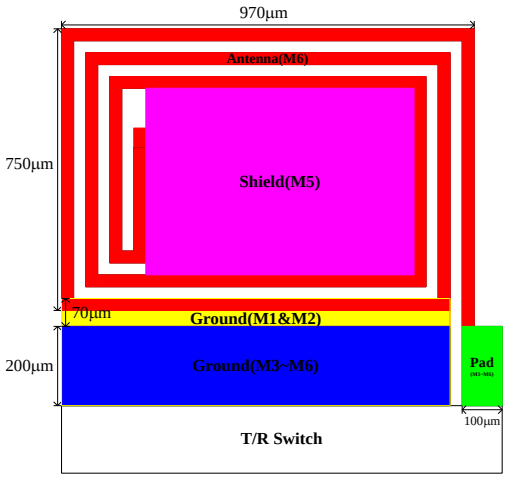

Fig. 2. Layout of 1.575 GHz and 2.4 GHz CMOS RFIC On-Chip Antenna and T/R-Switch.

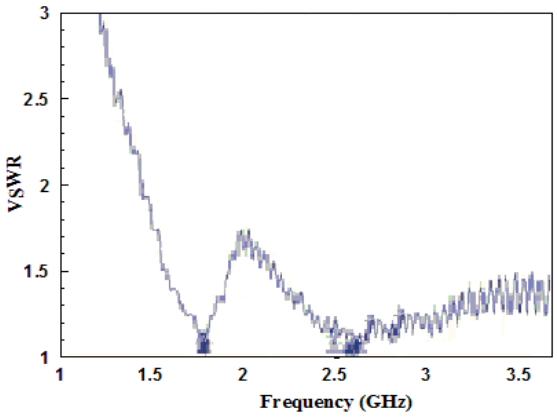

Fig. 3. Measured RFIC-on-Chip combo antenna VSWR.

Radiation Patterns of XY-Plane @ 2.45 GHz

XY plane	Max	Min	Average
E_ϕ gain (dBi)	-43.2	-38.7	-53.2
E_θ gain (dBi)	-61.4	-89.8	-67.4

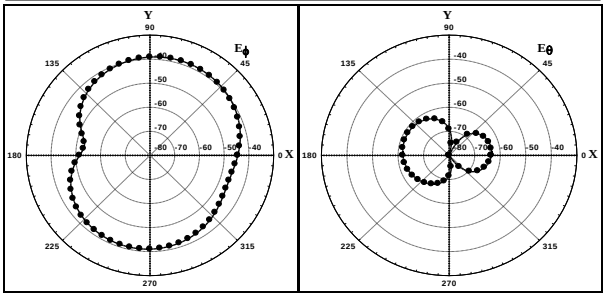

(a) E_ϕ-field (cross-polarization) (b) E_θ-field

Radiation Patterns of XZ-Plane @ 2.45 GHz

Xz plane	Max	Min	Average
E_ϕ gain (dBi)	-44.4	-53.0	-49.4
E_θ gain (dBi)	-40.9	-66.9	-46.1

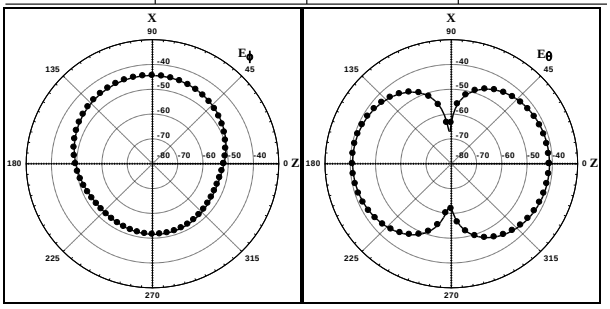

(a) E_ϕ-field (cross-polarization) (b) E_θ-field

Radiation Patterns of YZ-Plane @ 2.45 GHz

Xz plane	Max	Min	Average
E_ϕ gain (dBi)	-39.1	-41.4	-40.5
E_θ gain (dBi)	-49.6	-80.0	-56.1

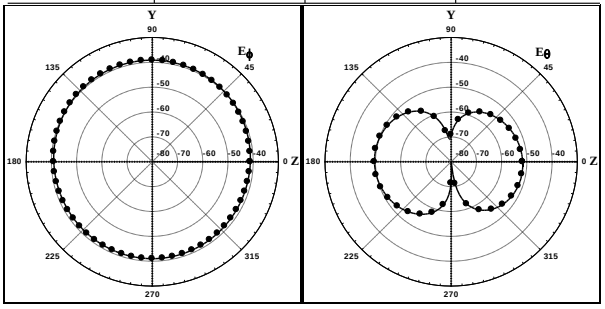

(a) E_ϕ-field (cross-polarization) (b) E_θ-field

Fig. 4. Measured antenna gain patterns.

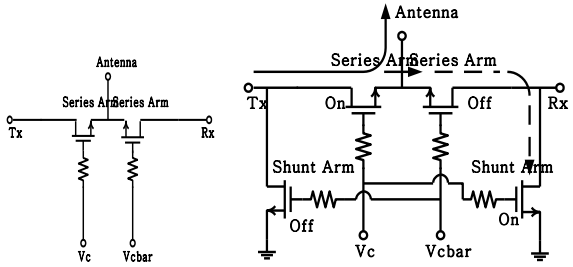

Fig. 5 T/R Switch architecture diagram and schematic.

III. T/R-SWITCH DESIGN

Regarding series type T/R Switch theory, this proposed voltage control series arm gate on transistors. The shunt/series type T/R Switch phase in shunt arm when shunt arm transistors switching on. Transistor gate width related on T/R switch phase in lost and isolation that means width increase and on-state resistance reduce then phase in lost as less. But opposite off-state capacitance increase and isolation go to bad. Base on TSMC support model design, series arm select 90/0.24um NMOS transistor, the control voltage V_c is

1.8V. After design simulation T/R-Switch circuit as shown in Fig. 6 and characteristics as shown in Table 1. R_1 connect to grounding means define DC voltage. R_2, R_3 is gate-level bias resistor. R_1, R_2 and R_3 are 20kΩ.

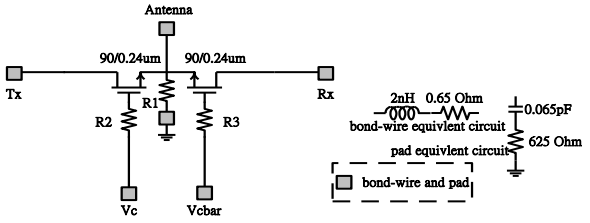

Fig. 6. T/R Switch circuit and layout.

Table 1: T/R Switch characteristics table

T/R Switch: Characteristics	
Control Voltage	1.8V
Insertion loss	<1.0dB
Input return loss (Tx and Rx modes)	>12dB
Input P_{1dB} (Tx and Rx modes)	>21dBm
Isolation (Tx-Rx in Tx mode)	>24dB
Isolation (ANT-Tx in Rx mode)	>18dB

IV. ELECTROMAGNETIC COUPLING BETWEEN ANTENNA AND HUMAN BODY

EM interaction between combo antenna and body are mutual coupling as shown in Fig. 7.

Expression of E field outside and inside a lossy body have confirm as shown in Fig. 8.

The EM interaction between antenna and body are B.C. and source model. Boundary condition on the perfectly conducting surface of the antenna as:

$$\hat{s}\cdot[\vec{E}^a(s)+\vec{E}^b(s)+\vec{E}^i(s)]=0, \quad (1)$$

$\vec{E}^a$ = electric field radiated from the combo antenna

$\vec{E}^b$ = electric field scattered from the induced current in the human body

$\vec{E}^i$ = impressed field from the voltage source.

(1) Delta-gap voltage source as shown in Fig. 9 (a):

$$E^i = V_o\delta(s)\cdot \quad (2)$$

(2) Magnetic frill source as shown in Fig. 9 (b):

$$\vec{M}_s = -\frac{2V_o}{\rho\ln(r_o/r_i)}\hat{\varphi}, \qquad \vec{E}^i = -\int_s \vec{M}_s\times\nabla'\frac{e^{-jk_oR}}{4\pi R}ds'. \quad (3)$$

According coupled integral equations (CIE), this proposed have calculated antenna IE and VEFIE with mutual coupling terms as shown in Fig. 10.

$$\frac{-1}{j\omega\varepsilon_o}\int_{ant}\left[\hat{s}\cdot\hat{s}'k_o^2 I(s')+\frac{\partial I(s')}{\partial s'}\cdot\frac{\partial}{\partial s}\right]G(s,s')ds' - \int_{V_b}\hat{s}\cdot\vec{\vec{G}}(s,\vec{r}')\cdot\tau(\vec{r}')\vec{E}(\vec{r}')dv' = \hat{s}\cdot\vec{E}^i(s)$$

$$\int_{ant} I(s')\hat{s}'\cdot\vec{\vec{G}}(\vec{r},s')ds' + PV\int_{V_b}\tau(\vec{r}')\vec{E}(\vec{r}')\cdot\vec{\vec{G}}(\vec{r},\vec{r}')dv' - \left[1+\frac{\tau(\vec{r})}{3j\omega\varepsilon_o}\right]\vec{E}(\vec{r}) = 0 \quad (4)$$

(1) Induced Equivalent Current Density as:

$$\vec{J}_{eq}(\vec{r}) = [\sigma + j\omega(\varepsilon-\varepsilon_o)]\vec{E}(\vec{r}) = \tau\vec{E}(\vec{r}). \quad (5)$$

(2) Dyadic Green's Function as:

$$\vec{\vec{G}}(\vec{r},\vec{r}') = -j\omega\mu_o[\vec{\vec{I}} + \frac{1}{k_o^2}\nabla\nabla]G(\vec{r},\vec{r}')$$

$$G(\vec{r},\vec{r}') = \frac{e^{-jk_o|\vec{r}-\vec{r}'|}}{4\pi|\vec{r}-\vec{r}'|}. \quad (6)$$

The proposed antenna with arbitrary orientation and wrist body are present as shown in Fig. 11 and Fig. 12 [8]-[12]. Regarding moment method (MoM) solution, the combo antenna current is expanded in terms of piecewise sinusoidal basis functions: (N_a segments) as:

$$I(\phi^*) = \sum_{n=1}^{Na} I_n f_n(\phi^*)$$

$$f_n(\phi^*) = \begin{cases} \dfrac{\sin(\phi^*-\phi^*_{n-1})}{\sin(\phi^*_n-\phi^*_{n-1})} & \text{if } \phi^*_{n-1}\le\phi^*\le\phi^*_n \\ \dfrac{\sin(\phi^*_{n+1}-\phi^*)}{\sin(\phi^*_{n+1}-\phi^*_n)} & \text{if } \phi^*_n\le\phi^*\le\phi^*_{n+1} \\ 0 & \text{otherwise} \end{cases} \quad (7)$$

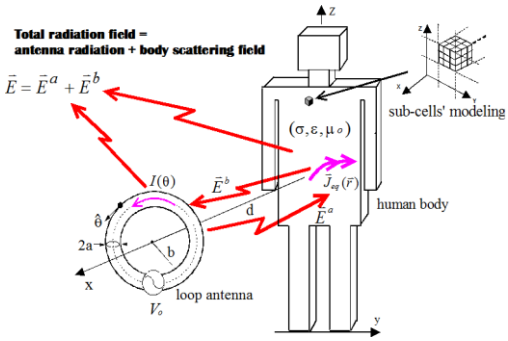

Fig. 7. EM interaction between antenna and body are mutual coupling.

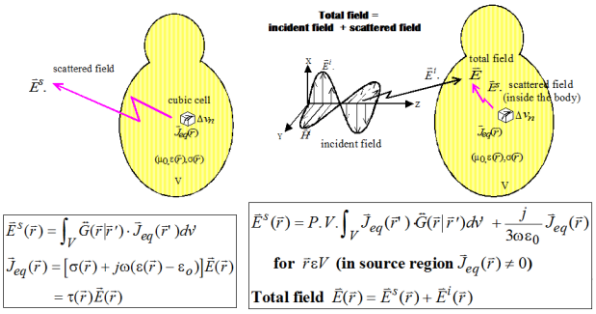

Fig. 8. Dyadic green's function technique.

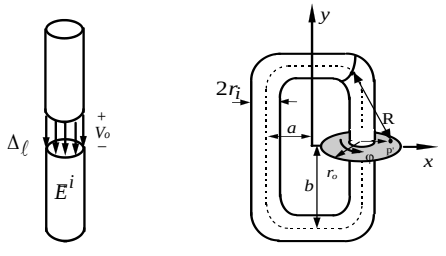

Fig. 9. (a) Delta-gap voltage source, and (b) Magnetic frill source.

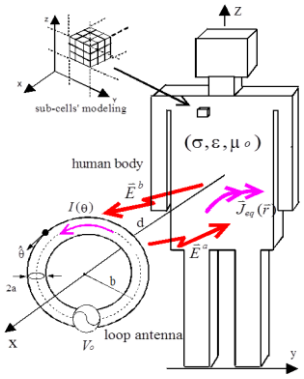

Fig. 10. Antenna IE and VEFIE with mutual coupling terms.

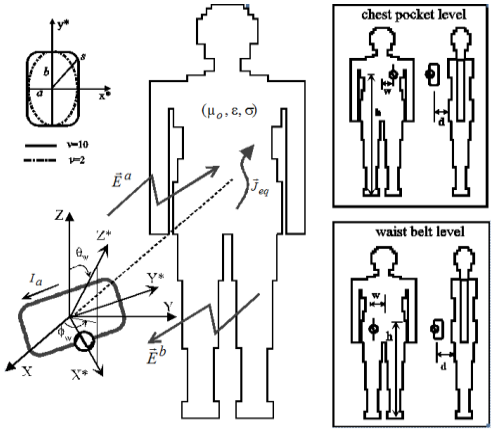

Fig. 11. Antenna with arbitrary orientation and wrist body.

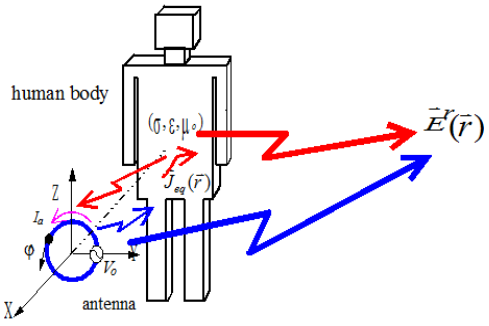

Fig. 12. Total radiation field from antenna and human body.

The induced electric field in the body is expressed in terms of pulse basis functions: (N_b cells) as:

$$\vec{E}(\vec{r}) = \hat{x}\sum_{n=1}^{N_b} E_x^n p_n(\vec{r}) + \hat{y}\sum_{n=1}^{N_b} E_y^n p_n(\vec{r}) + \hat{z}\sum_{n=1}^{N_b} E_z^n p_n(\vec{r}). \quad (8)$$

Moment Method Solution: Galerkin & point-matching as:

$$\frac{-1}{j\omega\varepsilon_o}\sum_{n=1}^{Na} I_n \int_{\phi^*_{m-1}}^{\phi^*_{m+1}}\int_{\phi^*_{n-1}}^{\phi^*_{n+1}} \left\{ (s_x{*}s'_x{*} + s_y{*}s'_y{*})k_o^2 f_n(\phi^{*\prime})\Delta(\phi^{*\prime}) - \frac{(jk_oR+1)}{R^2}\left[s_x{*}(x^{*}-x^{*\prime}) + s_y{*}(y^{*}-y^{*\prime})\right] \right.$$
$$\left. \frac{\partial f_n(\phi^{*\prime})}{\partial \phi^{*\prime}} \right\} \frac{e^{-jk_oR}}{4\pi R} f_m(\phi^*)\Delta(\phi^*) d\phi^{*\prime} d\phi^*$$
$$-\sum_{n=1}^{N_b}\sum_{p=1}^{3} E_{x_p}^n \int_{V_b} \tau_n \int_{\phi^*_{m-1}}^{\phi^*_{m+1}} \left[s_x G_{xx_p}(s,r') + s_y G_{yx_p}(s,r') + s_z G_{zx_p}(s,r') \right] f_m(\phi^*)\Delta(\phi^*) d\phi^* dv'$$
$$= \int_{\phi^*_{m-1}}^{\phi^*_{m+1}} (s_x{*}\hat{x}^{*} + s_y{*}\hat{y}^{*}) \cdot \vec{E}^i(\phi^*) f_m(\phi^*)\Delta(\phi^*) d\phi^* \quad (9)$$

$$\sum_{p=1}^{3} \hat{x}_p \left\{ \sum_{n=1}^{N_a} I_n \int_{\phi^*_{n-1}}^{\phi^*_{n+1}} \left[G_{x_px}(\vec{r}_i, s')s_x + G_{x_py}(\vec{r}_i, s')s_y + G_{x_pz}(\vec{r}_i, s')s_z \right] f_n(\phi^{*\prime})\Delta(\phi^{*\prime}) d\phi^{*\prime} \right.$$
$$\left. + \sum_{n=1q=1}^{N_b}\sum^{3} E_{x_q}^n \left[\tau_n \mathrm{PV}. \int_{(\Delta v)_n} G_{x_px_q}(\vec{r}_i, \vec{r}')dv' - \delta_{pq}\delta_{\vec{r}_i\vec{r}_n}\left(1 + \frac{\tau_i}{j3\omega\varepsilon_o}\right) \right] \right\} = 0 \quad (10)$$

Finally moment method solution is transformation of CIEs to matrix equation as:

$(N_a + 3N_b) \times (N_a + 3N_b)$ matrix equation:

$$\begin{bmatrix} [AA] & [AB^x] & [AB^y] & [AB^z] \\ [BA^x] & [BB^{xx}] & [BB^{xy}] & [BB^{xz}] \\ [BA^y] & [BB^{yx}] & [BB^{yy}] & [BB^{yz}] \\ [BA^z] & [BB^{zx}] & [BB^{zy}] & [BB^{zz}] \end{bmatrix} \begin{bmatrix} [I_a] \\ [E_b^x] \\ [E_b^y] \\ [E_b^z] \end{bmatrix} = \begin{bmatrix} [V^i] \\ [0] \\ [0] \\ [0] \end{bmatrix}, \quad (11)$$

[AA]: $N_a \times N_a$ submatrix (antenna to antenna),

[AB]: $N_a \times 3N_b$ submatrix (body to antenna),

[BA]: $3N_b \times N_a$ submatrix (body to antenna),

[BB]: $3N_b \times 3N_b$ submatrix (body to body),

$[I_a]$: N_a column-vector (antenna current),

$[E_b^\alpha]$: N_b column-vector (a component of the induced field in the body).

Total radiation field from antenna and human body as:

$$\vec{E}^r(\vec{r}) = -j\eta_o k_o \frac{e^{-jk_or}}{4\pi r}\int_{-\pi}^{\pi} \left\{ \hat{\theta}[-I(\theta')\sin\theta'\cos\theta\sin\phi - I(\theta')\cos\theta'\sin\theta] + \hat{\phi}[-I(\theta')\sin\theta'\cos\phi] \right\}$$
$$e^{jk_o(x'\sin\theta\cos\phi + y'\sin\theta\sin\phi + z'\cos\theta)} b d\theta' \quad \textbf{loop antenna radiation field}$$
$$-j\eta_o k_o \frac{e^{-jk_or}}{4\pi r}\int_{V_b} \left\{ \hat{\theta}[J_{eq}^x(\vec{r}')\cos\theta\cos\phi + J_{eq}^y(\vec{r}')\cos\theta\sin\phi - J_{eq}^z(\vec{r}')\sin\theta] + \right.$$
$$\left. \hat{\phi}[-J_{eq}^x(\vec{r}')\sin\phi + J_{eq}^y(\vec{r}')]\cos\phi \right\} e^{jk_o(x'\sin\theta\cos\phi + y'\sin\theta\sin\phi + z'\cos\theta)} dv'$$
$$\textbf{body-induced current radiation field} \quad (12)$$

The antenna parameters (affected by body) as shown in Fig. 14 and below:

(1) Input power & input impedance:

$$P_i = \tfrac{1}{2}\mathrm{Re}\left[V_o I_o^*\right], \quad Z_i = V_o / I_o.$$

(2) Power absorbed by body:

$$P_{abs} = \int_{V_b} \tfrac{1}{2}\sigma |\vec{E}|^2 \, dv.$$

(3) Power radiated to free space:

$$P_{rad} = \oint_s \tfrac{1}{2}[\vec{E}^r \times \vec{H}^{r*}] \cdot d\vec{s}.$$

(4) Directive gain:

$$G(\theta,\phi) = \frac{\tfrac{1}{2}\mathrm{Re}[\vec{E}^r \times \vec{H}^{r*}]}{P_{rad}/(4\pi r^2)}.$$

(5) Radiation efficiency:

$$\eta_{rb} = \frac{P_{rad}}{P_{rad} + P_{abs}} \text{(body absoption)} \quad \eta_{r\Omega} = \frac{R_r}{R_r + R_{ohm}} \text{(ohmic loss)}.$$

(6) Power gain:

$$G_p = \eta_{rb} \times \eta_{r\Omega} \times G.$$

(7) Average G_p:

$$G_{avg} = \frac{1}{8}\sum_{i=1}^{8} G_p(\theta = \tfrac{\pi}{2}, \phi_i).$$

(8) Receiving system noise temperature:

$$T_{sys} = T_A + T_{REC}.$$

(9) Antenna noise temperature: T_A,

(T_b: **background noise temperature**),

$$T_A = \eta_{r\Omega} T_b + (1 - \eta_{r\Omega}) T_P,$$

only $\eta_{r\Omega}$ (not η_{rb}) appear in T_A.

Rectangular combo antennas of y-orientation at 2.4 to 2.483 GHz measured results as shown in Fig. 13 and below Table 2. The 3D patterns of rectangular combo antennas as shown in Fig. 14-Fig. 18 [8]-[12].

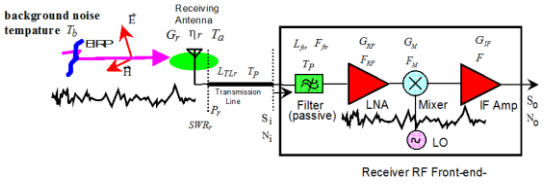

Fig. 13. Antenna and receiving system S/N Ratio (affected by body).

Table 2: Rectangular combo antennas of y-orientation at 2.4 GHz

Antenna Position	in free space	chest pocket level	waist belt level
E_θ Max. Power Gain (dB)	-12.4	-7.4	-8.6
E_θ Min. Power Gain (dB)	-22.3	-56.8	-34.0
E_θ Ave. Power Gain (dB)	-15.0	-13.4	-13.6
E_ϕ Max. Power Gain (dB)	<-100	-20.8	-21.3
E_ϕ Min. Power Gain (dB)	<-100	-38.5	-41.3
E_ϕ Ave. Power Gain (dB)	<-100	-23.7	-25.7

Antenna Position	Free Space	Chest Pocket Level			Waist Belt Level
Antenna Orientation	Y	X	Y	Z	Y
Radiation Efficiency $\eta_{r\Omega}$	4	33	17	26	14
Radiation Efficiency η_{rb}	100	13	40	27	45
Total Efficiency (%)	4	4.29	6.8	7	6.3
Nosie Temperature(K)**	296	267	283	274	286

* **Total Radiation Efficiency** $\eta_r = \eta_{r\Omega} \times \eta_{rb}$

** $T_A = \eta_{r\Omega} T_b + (1 - \eta_{rr\Omega}) T_{p_r}$,
assuming T_b=200 K & T_p=300 K

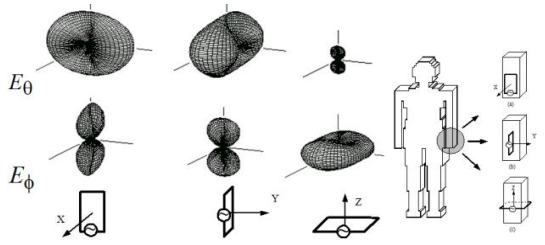

Fig. 14. 3D patterns of rectangular combo antennas in free space (1.575 GHz).

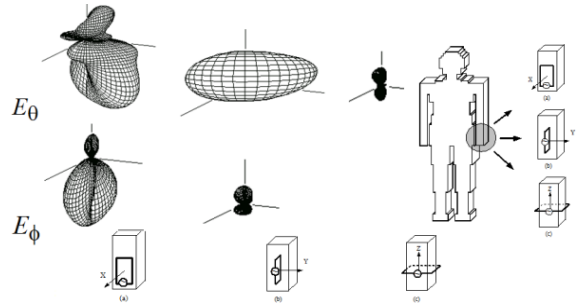

Fig. 15. 3D patterns of rectangular combo antennas at the Wrist (1.575 GHz).

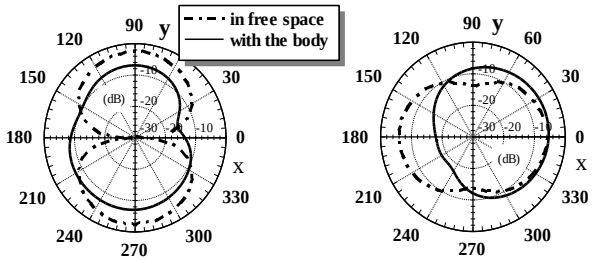

Fig. 16. 2D power patterns in the H-plane at wrist level (1.575 GHz).

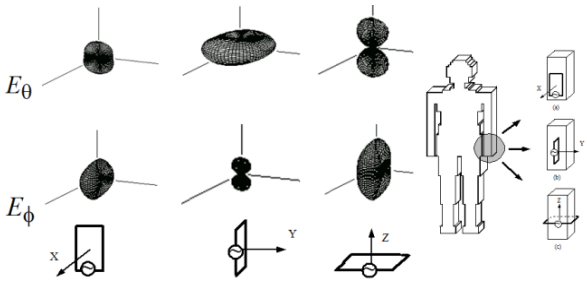

Fig. 17. 3D patterns of rectangular antennas in free Space (2.45 GHz).

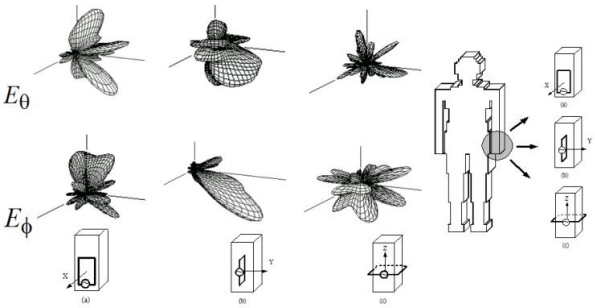

Fig. 18. 3D patterns of rectangular combo antennas at the wrist (2.45 GHz).

Detailed analysis and extensive numerical simulations of the influence of a human body model on combo antennas with arbitrary orientations for personal

wireless communications has been conducted. Coupled integral equations (CIE), which consist of a Pocklington-type integral equation (PIE) and a volume electric field integral equation (VEFIE) with mutual coupling terms, and the method of moments (MoM) are used to numerically solve this antenna-body coupling problem. The proximate human body absorbs a large part of the antenna radiated power and reduces the antenna radiation efficiency. For the circular combo antenna: (2.45 GHz) as:

x- : body-absorption & ohmic-loss efficiency η_{rb}=5%, $\eta_{r\Omega}$=69%, η_r=3.5%
y- : body-absorption & ohmic-loss efficiency η_{rb}=62%, $\eta_{r\Omega}$=44%, η_r=27.5%
z- : body-absorption & ohmic-loss efficiency η_{rb}=25%, $\eta_{r\Omega}$=58%, η_r=14.6%.

For the rectangular combo antenna: (2.45 GHz) as:

x- : body-absorption & ohmic-loss efficiency η_{rb}=13%, $\eta_{r\Omega}$=33%, η_r=4.3%
y- : body-absorption & ohmic-loss efficiency η_{rb}=40%, $\eta_{r\Omega}$=17%, η_r=6.8%
z- : body-absorption & ohmic-loss efficiency η_{rb}=27%, $\eta_{r\Omega}$=26%, η_r=7.0%.

The EM coupling effects of the human body increase the radiation resistance (rectangular part of input impedance) for 4 to 10 times for different orientations, and hence, enhance the antenna ohmic-loss efficiency. The average power gain in the H-plane for the y-oriented combo antenna, a preferred choice for general pager usage, is enhanced about 2 dB by the human body. For watch-type communicator applications, the (z-oriented) combo antenna encircling the wrist may be a preferred choice. Numerical results of the antenna input impedance, radiation patterns, cross-polarization field level, radiation efficiencies, and maximum/minimum/average power gains are important for the pager or wireless communicator antenna/RF design and communication link budget consideration. Numerical simulation of complicated antenna parameter variations is important for the pager antenna/RF design and communication link budget consideration. For watch-type communicator applications, the (z-oriented) combo antenna encircling the wrist may be preferred choice. Numerical results of the antenna input impedance, radiation patterns, cross-polarization field level, radiation efficiencies, and maximum/minimum/average power gains are important for the pager or wireless communicator antenna/RF design and communication link budget consideration. Detailed near-zone behavior of the E-field distribution of the combo antenna is also studied for EMC application. The superquadric antenna is used to model the signal trace on the FPC board. The radiation efficiency of higher-order harmonic frequencies from a rectangular antenna to free space is not necessarily higher than that of lower frequencies. The proximate human body absorbs a large part of the radiated power from the combo antenna and reduces the antenna radiation efficiency:

x- : absoption = 87% radiation efficiency η_{rb}=13%
y- : absoption = 60% radiation efficiency η_{rb}=40%
z- : absoption = 73% radiation efficiency η_{rb}=27%.

The EM coupling effects of the human body increase the radiation resistance (real part of input impedance) for 5 to 10 times for different orientations and hence enhance the antenna ohmic-loss efficiency. The average power gain in the H-plane for the y-oriented combo antenna is enhanced about 2 dB by the human body. For watch-type communicator applications, the (z-oriented) combo antenna encircling the wrist may be preferred choice. Numerical results of the antenna input impedance, radiation patterns, cross-polarization field level, radiation efficiencies, and maximum/minimum/average power gains are important for the pager or wireless communicator antenna/RF design and communication link budget consideration. Detailed near-zone behavior of the E-field distribution of the combo antenna is also studied for EMC application. The superquadric antenna is used to model the signal trace on the FPC board. The radiation efficiency of higher-order harmonic frequencies from a rectangular antenna to free space is not necessarily higher than that of lower frequencies. Analysis and extensive numerical computation of EM interaction between a human body model and a circular combo antenna with arbitrary orientation for radio paging communications has been performed. The proximate human body absorbs a large part of the antenna radiated power and reduces the antenna radiation efficiency, but enhance the radiation resistance (real part of input impedance), and hence, increase the antenna ohmic-loss efficiency:

x- : body-absoption & ohmic-loss efficiency η_{rb}=6% $\eta_{r\Omega}$=70%
y- : body-absoption & ohmic-loss efficiency η_{rb}=61% $\eta_{r\Omega}$=46%
z- : body-absoption & ohmic-loss efficiency η_{rb}=26% $\eta_{r\Omega}$=60%.

As the electromagnetic spectrum becomes more crowded and the digital hardware is widely used, it is important for engineers to take electromagnetic interference into account in the circuit design process. Because EMC equipment operate normally in proximity to other electronic devices, it is important that the near field distribution of the antenna must be carefully quantified. In EMC analysis, radiated emissions from signal traces in FPC boards are an important topic. In some situation, the signal trace encloses to an antenna. It is known that an antenna having small perimeter compared to a wavelength is an inefficient radiating element. However, when the signal frequency is high enough, the electrical perimeter of the antenna may then be comparable to a wavelength. The antenna will become an efficient radiator. In addition, detailed near-zone behavior of the E-field distribution of the combo antennas is studied for electromagnetic compatibility (EMC) application. The superquadric antenna is used to model the signal trace on the FPC board. A circular, rectangular, and elliptical antennas have are studied. The E-field distribution of the rectangular antenna in the near-zone region, which corresponded to the fundamental frequency, 2nd and 3rd harmonics of a clock rate, are computed. It is found that the radiation efficiency of higher-order harmonic frequencies from a rectangular antenna to free space is not necessarily higher than that

of lower frequencies. Numerical results may be useful for the analysis of radiated emission of the signal trace on a FPC board.

V. GPS FIELD TRIED MEASURED RESULTS

For GPS static and dynamic evaluation, this antenna performance criteria are carry per noise ratio more than 40 (C/N >= 40) and TTFF less than 45 seconds under signal generator by antenna with wireless device. This wearable ambulatory application also provide GPS field trial test at multi-difficult conditions such as high building, high tree, high bridge, alley, underground tunnel by dead reckoning for mobile biomedical application. Normally the old man can monitor healthcare and transfer to health center by Miracast with software and show GPS location. Even ambulance goes to hospital on the way also can simulations such as freeway shown as in Fig. 19.

Fig. 19. GPS antenna filed tried measurement at freeway.

VI. CONCLUSION

This paper has provided COMS RFIC On-Chip combo antenna with T/R Switch design to support wrist wearable ambulatory technological performance and mobile biomedical healthcare application.

REFERENCES

[1] E. Ojefors, F. Bouchriha, K. Grenier, and A. Rydberg, "24 GHz ISM-Band Antennas on Surface Micro-machined Substrates for Integration with a Commercial SiGe Process," Department of Engineering Sciences, Uppsala University, Uppsala, Sweden.

[2] http://www.eettaiwan.com

[3] Electronic Engineering Times-Taiwan, pp. 3, Nov. 15, 2003.

[4] F.-J. Huang and O. Kenneth, "A 0.5-um CMOS T/R switch for 900-MHz wireless applications," *IEEE Journal of Solid-State Circuits*, vol. 36, no. 3, pp. 486-492, Mar. 2001.

[5] K. Yamamoto, T. Heima, A. Furukawa, et al., "A 2.4-GHz-band 1.8-V operation single-chip Si-CMOS T/R-MMIC front-end with a Low insertion loss switch," *IEEE Journal of Solid-State Circuits, v*ol. 36, no. 8, pp. 1186-1197, Aug. 2001.

[6] M. R. Kamarudin, Y. I. Nechayev, and P. S. Hall, "Antenna for on-body communication systems," *IEEE IWAT*, pp. 17-20, Mar. 2005.

[7] J.-F. Huang, J.-Y. Wen, and W.-C. Lai, "Design of a printed dipole array antenna with wideband power divider and RF switches," *Microwave and Optical Technology Letters*, vol. 55, no 10, pp. 2410-2413, Oct. 2013.

[8] J.-F. Huang and W.-C. Lai, "Design of a compact printed double-sided dual-band dipole antenna by Fdtd for Wifi application," *Microwave and Optical Technology Letters*, vol. 55, pp. 1845-1851, Aug. 2013.

[9] W.-C. Lai and J.-F. Huang, "Numerical modeling of electromagnetic coupling electronic device with proximity-based radio power control for LTE/ WWAN SAR," *IEEE Fifth International Conference on Advanced Computational Intelligence (ICACI)*, pp. 142-147, Oct. 18-20, 2012.

[10] J.-F. Huang, W.-C. Lai, and P.-G. Yang, "An automatically tuneable antenna design with GPS dead reckoning switch for multiband laptop and mobile cellular phone applications to the human body," *The 2013 6th International Conference on BioMedical Engineering and Informatics (BMEI)*, pp. 306-311, Dec. 16-18, 2013.

[11] "A 2.4-GHz RFIC-on-chip antenna on flexible surface proximate to the human body for miracast and wireless application," *International Workshop on Microwave and Millimeter Wave Circuits and System Technology (MMWCST)*, pp. 165-169, Oct. 24-25, 2013.

[12] "Long term evolution antenna design by FDTD for Femto communication on tablet application," *International Microwave Workshop Series on RF and Wireless Technologies for Biomedical and Healthcare Applications (IMWS-Bio 2015)*, pp. 120-121, Sep. 21-23, 2015.

Wen-Cheng Lai received Ph.D. degrees in Electronic Engineering from National Taiwan University of Science and Technology in 2015. He is Hardware Director in ASUSTek Computer Inc. Taiwan.

Jhin-Fang Huang received Ph.D. degrees in Electrical Engineering from University of Kansas, U.S.A. From 1989-Now he is Associate Professor in Department of Electronic Engineering National Taiwan University of Science and Technology.